Multiple Scattering Calculations of Bonding and X-ray Absorption Spectroscopy of Manganese Oxides

B. Gilbert,*,† B. H. Frazer,†,‡ A. Belz,§ P. G. Conrad,§ K. H. Nealson,§ D. Haskel,|| J. C. Lang,|| G. Srajer,|| and G. De Stasio†

Department of Physics, and Synchrotron Radiation Center, University of Wisconsin, 3731 Schneider Drive, Stoughton, Wisconsin 53589, Institut de Physique Appliquee, Ecole Polytechnique Federal de Lausanne, Jet Propulsion Laboratory, Pasedena, California, and Advanced Photon Source, Argonne National Laboratory, Argonne, Illinois 60439

Received: June 25, 2002; In Final Form: December 5, 2002

We present near edge X-ray absorption spectra of manganese oxides at the Mn $L_{2,3}$, Mn K, and O K edges to investigate the relative sensitivity of the edges to bonding and structure. Collectively, the spectra probe local electronic structure and intermediate range crystal structure. Spin independent full multiple scattering calculations of the Mn K edge give good agreement with data above threshold and qualitatively reproduce the prepeak that is observed for each compound. We show that the apparent prepeak for MnO is not due to p−d hybridization at the Mn atom (in accordance with symmetry principles) or quadrupolar transitions but originates from multiple scattering within the fifth shell. We present spin dependent multiple scattering calculations of the O K edge and show that this edge allows for a more direct description of the 3d states than either the Mn L edge or K edge prepeak, which are complicated by multiplet effects.

1. Introduction

The particularly rich redox chemistry of manganese is evident in its oxides, which are of wide contemporary interest in the physical and environmental sciences. The sensitivity of X-ray absorption near edge structure (XANES) spectroscopy to local structure and valence has been used to study manganese in manganese oxide cathodes[1] and colossal magnetoresistant (CMR) materials,[2−4] enzymes,[5] environmental precipitates,[6] and minerals.[7] There are two specific areas for which XANES analysis is anticipated to remain of great value. First, many technological[9] and environmental[10] occurrences of Mn are in nanosize material, for which bulk methods of chemical analysis are challenged.

A further area of growth is chemical analysis at a submicron scale, e.g., microchemical inhomogeneities in manganite films[11] or inclusions in geological specimens.[12] X-ray microscopes that can perform XANES spectroscopy (spectromicroscopes) are now installed on several synchrotron sources, with a lateral resolution reaching 20 nm.[13,14] X-ray absorption is inherently higher in energy resolution than electron energy-loss spectroscopy (EELS) and has analyzed hydrated environmental specimens.[15,16] Thus, there is the possibility of performing high *spatial* and *energy* resolution microchemical analysis of complex specimens.

High quality reference spectra of characterized bulk material and an established interpretation are required as a foundation for studies on low dimensional or complex systems. A number of excellent compilations of manganese oxide XANES spectra at a single absorption edge are available in the literature.[17,18] However, not all are at the highest energy resolution, and there are some discrepancies in absolute energy position as well as energy axis scaling at the Mn K edge,[19,20] ambiguous line shapes for different Mn valences at the Mn L edge,[21] and oxidized MnO specimens.[22,23] We present XANES of Mn oxide standards acquired on high-resolution synchrotron beamlines. A particular effort has been made to ensure the purity of the compounds and the veracity and energy position of all X-ray absorption spectra, by ensuring beamline calibration and comparing with earlier XANES and EELS data, and to calculations in the literature and performed here.

Although the fundamentals of X-ray absorption are well established, numerical simulation of XANES spectra remains far from routine because of the complexity of the process. The key step is the relation of the absorption cross section to the density of unoccupied electronic states. The real space multiple scattering approach of the FEFF code has been extended to the near edge region by simulating full multiple scattering (FMS) of the photoelectron from atomic sites,[24] and calculations of XANES have been very successful for both metallic and semiconducting materials,[24,25] despite neglect of nonspherical contributions to the electrostatic potentials. We perform XANES calculations for Mn and O K edges of the compounds studied here, including spin-dependent calculations at the O K edge to account for the spin-split d bands. Incorrect treatment of the exchange correlation for the d orbitals means that Mn L edge absorption cannot be successful simulated. Nevertheless, there is much of value in this approach, in particular the direct link between local crystal structure and Mn and O K edge XANES, which is fully examined to reveal aspects of X-ray absorption spectroscopy of these systems that cannot be reproduced by current full potential methods.

* To whom correspondence should be addressed. Present address: Department of Earth and Planetary Sciences, University of California−Berkeley, 455 McCone Hall, CA 94720. E-mail: bgilbert@eps.berkeley.edu.
† University of Wisconsin.
‡ Ecole Polytechnique Federal de Lausanne.
§ Jet Propulsion Laboratory.
|| Argonne National Laboratory.

10.1021/jp021493s CCC: $25.00
Published on Web 03/29/2003

TABLE 1: Manganese Oxides Selected for This Study

compound	name	crystal class, space group	Mn site symmetry	Mn formal valence	Mn−O bond length/Å[a]	d-band occupancy[b]
$KMnO_4$	potassium permanganate	orthorhombic P n m a	tetrahedral	+7	1.543−1.559 (1.55)[c]	$3d^0$ $\uparrow t_2^0$
MnO_2	pyrolusite	tetragonal P 4_2/mnm	dis. oct	+4	1.877−1.891 (1.886)[c]	$3d^3$ $\uparrow t_{2g}^3$
Mn_3O_4	hausmannite	tetragonal l 4/amd	dis. text. dis. oct.	+2 +3		− −
Mn_2O_3	bixbyite	cubic l a-3	oct. dis. oct.	+3 +3	1.993 1.899−2.248 (2.019)[c]	$3d^4$ $\uparrow t_{2g}^3 e_g^1$
MnO	manganosite	cubic f m-3 m	oct.	+2	2.222	$3d^6$ $\uparrow t_{2g}^3 e_g^2$

[a] Bond length data are taken from ref 26. [b] Given are the occupancies with atomic orbital designation as well as ground-state crystal field orbitals, assuming perfect O_h symmetry. [c] Values in parentheses are the average.

2. Experiment and Theory

X-ray Absorption Spectroscopy. The reference manganese oxides listed in Table 1 were purchased from Aldrich and checked by X-ray powder diffraction (XRD). Manganese (II) oxide pieces (Aldrich, packaged in argon) were handled under a nitrogen atmosphere, ground and pressed onto indium metal, and transferred to the vacuum system with minimal exposure to oxygen. Despite anaerobic handling, the X-ray absorption experiments detected surface oxidation of MnO (XRD did not detect this surface oxidation). Argon ion sputtering for a total of 60 min with a 1 kV accelerating potential and at $<1 \times 10^{-6}$ Torr pressure substantially removed this surface oxidation. As the specimen was powdered for data acquisition, the sputtering effectiveness was inevitably limited; nevertheless, an excellent L edge absorption spectrum of Mn^{2+} was recorded, and a reasonable quality O K edge absorption spectrum was obtained as described below. The other manganese oxides were not found to be sensitive to oxidation and were handled in air, powdered, and pressed onto conducting carbon tape.

Mn L edge and O K edge absorption spectroscopy of reference manganese oxide compounds was performed on the HERMON beamline of the University of Wisconsin Synchrotron Radiation Center (UW−SRC). Data were acquired in total electron yield mode, measuring the photocurrent emitted from the specimen surface by a picoammeter connected to the sample holder. The carbon tape was free from manganese, and after coating by the reference powders, no oxygen signal from the tape was detected in any Mn oxide spectra. For Mn L edge spectroscopy, the photon energy resolution was 0.1 eV. For O K edge spectroscopy, the photon energy resolution was 0.2 eV.

Two measures were taken to ensure consistent grating energy calibration. The Mn_2O_3 specimen was treated as an internal calibration standard, and this Mn L edge spectrum was reacquired prior to all other absorption edges to ensure no offsets in energy calibration. Additionally, all Mn L and all O K edge spectra sets (with the exception of MnO and $KMnO_4$) were each acquired in a single synchrotron fill to reduce the possibility of electron beam displacements affecting beamline monochromator energy calibration.

Mn K edge absorption spectroscopy was performed in beamline 4-ID-D at the Advanced Photon Source, Argonne, in transmission geometry. Powders of the reference compounds were brushed onto tape and stacked to achieve an edge jump of approximately 1 absorption unit. The monochromator was calibrated to the absorption edge of Mn foil, and the XANES spectra acquired at a resolution of better than 0.5 eV.

X-ray Absorption Calculations. We performed calculations of Mn K edge X-ray absorption spectra of selected manganese oxides with version 8 of the real space, full multiple scattering FEFF code.[24] The atomic coordinates were generated by ATOMS 3.0 using crystallographic input parameters from ref 26. The following FEFF calculation parameters best reproduced the Mn K edge data. The spherically symmetric muffin tin potentials were calculated self-consistently over a 5.0−5.3 Å radius, corresponding to three closest shells, up to the $l = 2$ angular momentum basis. The default overlapping muffin tin potentials were used, as this is considered a better approximation to the non spherical charge distribution in these compounds.[27] The calculated X-ray absorption transitions were to fully relaxed excited states in the presence of a core hole and with the Hedin−Lunqvist exchange-correlation potential.

The energy position of the Fermi level derived by the spin independent self-consistent potential calculations does not adequately describe the valence electronic structure in these compounds. As explained in more detail below, because of the neglect of spin dependent exchange effects, the d band occupations predicted by FEFF are incorrect. To allow a qualitative description of preedge absorption at the Mn K edge, X-ray absorption spectra were calculated with completely empty d bands. This was achieved in FEFF by applying a 2 eV energy shift to locate the Fermi level below the crystal field split d bands that are in reality partly filled. This approach does not affect the electronic structure calculations but simply shifts the absorption threshold so that transitions to all 3d states are considered. This allows an evaluation of p−d hybridization at the metal atom. We verified that this shift did not affect the self-consistent calculation of the potentials. Spin dependent calculations were performed to describe oxygen K edge absorption, as described below.

For structures with two distinct Mn sites (Mn_2O_3 and Mn_3O_4; see Table 1) full calculations were performed for each absorber, and the results combined according to stoichiometry. The cluster radii for full multiple scattering were 8 Å ($KMnO_4$, 131 atoms); 5.7 Å (MnO2, 91 atoms); 6.2 and 6.24 Å (Mn_3O_4, 89 and 85 atoms); 5.8 Å (Mn_2O_3, 75 and 78 atoms); 6.0 Å (MnO, 81 atoms). To compare experimental and calculated spectra, a 1 eV rigid shift to lower energy was applied to each calculated spectrum. To achieve a reasonable agreement with experimental peak intensities on the main edge, we set the X-ray absorption amplitude reduction factor $S_o^2 = 0.8$, included thermal disorder with a Debye temperature of 350−650 K, and added a 0.25−1.5 eV broadening to the calculations (applied above threshold only to avoid excessive broadening in the prepeak region).

Selected oxygen K edge spectra were calculated with the same parameters as for the Mn K edge, using FEFF version 8.10d. The spin resolved density of states were calculated indepen-

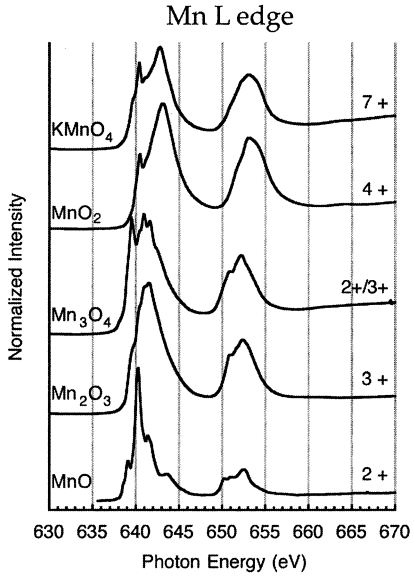

Figure 1. Manganese L edge X-ray absorption spectra of the samples given in Table 1. The formal Mn oxidation states are given on the right.

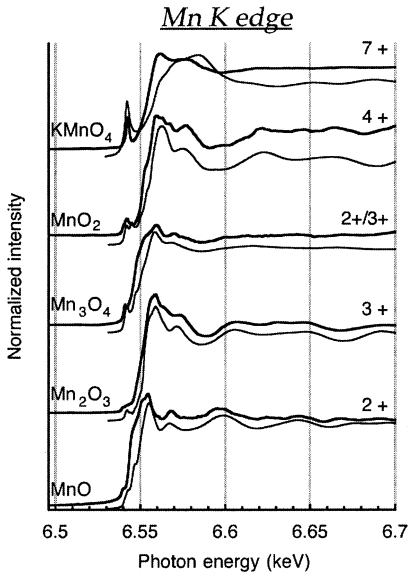

Figure 2. Manganese K edge X-ray absorption spectra (upper, thick curves) of the samples given in Table 1, compared with full multiple scattering calculations (lower, thin curves).

dently and non self-consistently (a present limitation of the code). This approach partially accounts for electron correlation by considering interactions only between parallel spins and has been widely applied in *X*α MS molecular orbital calculations.[28,29] As photoabsorption is spin-conserving, the spin up and spin down X-ray absorption spectra were obtained separately and summed.

Angular momentum projected densities of states are also presented to aid interpretation of the data. Comparisons between FEFF MS ground-state calculations for MnO and molecular orbital predictions were made with Sherman's *X*α-MS calculations of MnO_6 clusters in pure O_h symmetry (with Mn−O distance of 2.21 Å (Mn^{2+}).[28] The molecular orbital data for the tetrahedral MnO_4 cluster in $KMnO_4$ was obtained from ref 30.

3. Results and Analysis

X-ray Absorption Spectroscopy of Reference Mn Oxides. Manganese L edge spectra for the minerals listed in Table 1 are given in Figure 1. Mn L edge spectra for a number of these minerals have been previously acquired with either X-ray absorption[17] or electron energy-loss spectroscopy (EELS).[18] The data presented here are equivalent in energy resolution to existing X-ray data and show considerably better resolution than any published EELS data. We include the first accurate MnO XANES spectrum, as the existence of surface oxidization was not realized in previous X-ray studies. The nature of the oxidization is discussed below. Despite the presence of two distinct Mn atom sites in Mn_2O_3, the spectrum is similar to published data of Mn 3+ in perfect octahedral symmetry.[17]

Manganese K edge spectra for the minerals listed in Table 1 are given in Figure 2, alongside simulated XANES spectra. For the calculations of Mn with valences 2+, 3+, and 4+, the principal absorption features observed in the data are reproduced by calculation, and the energy distance between the prepeak and later absorption features is well reproduced. The main edge and prepeak calculations are discussed in more detail below. Oxygen K edge spectra for the minerals listed in Table 1 are given in Figure 3. The results of calculation for selected compounds are displayed in subsequent figures.

MnO Surface Oxidation. Figure 4 a shows the Mn L edge of powdered MnO before and after 1 h Ar ion sputtering. The final

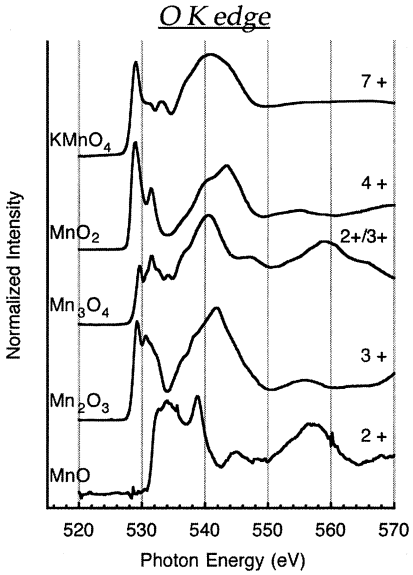

Figure 3. Oxygen K edge X-ray absorption spectra of the samples given in Table 1. The first absorption features, between 528 and 535 eV, are charge-transfer transitions to Mn d states. The subsequent features are transitions to metal−oxygen sp states.

line shape matches the spectrum of $MnSO_4$ (not shown), another Mn 2+ compound with manganese octahedrally complexed by oxygen. The subtraction of the sputtered MnO spectrum from the original reveals a very close match to the Mn_2O_3 spectrum, indicating that Mn 3+ is the sole product of room-temperature surface oxidation. Studies of aqueous Mn 2+ oxidation have shown that Mn_3O_4 is the initial product, but with the surface dominated by Mn 3+,[36] consistent with our observation.

The oxygen spectrum of the same specimen also evolved with sputtering, in particular with a reduction in prepeak intensity (marked by an arrow in Figure 4 b). However, the prepeak remained after sputtering, indicating persistent contamination. The true O K edge spectrum was obtained by scaling the original spectrum (assumed to show only the contamination signal) so that the prepeak intensity coincided with the 1 h sputtering curve (contamination plus true signal). Taking the difference revealed the true MnO spectrum, in excellent agreement with EELS

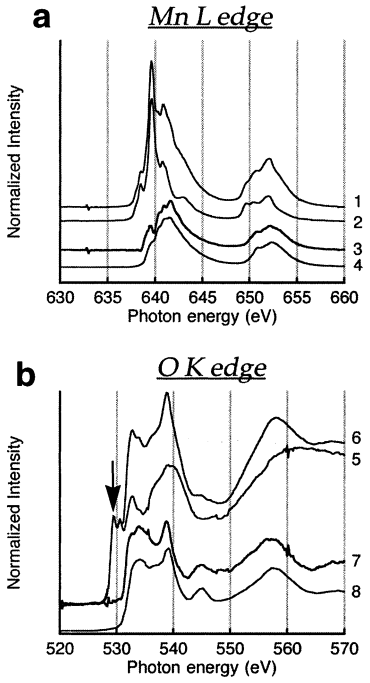

Figure 4. Surface oxidation of MnO was detected at (a**)** the Mn L edge (spectrum labeled 1) and (b**)** the O K edge (spectrum 5). After Ar ion sputtering, the true MnO spectrum was revealed at the Mn L edge (spectrum 2). Taking the difference (spectrum 3) revealed the surface layer to be Mn 3+ (by comparison with Mn_2O_3, spectrum 4). Oxygen-containing surface contamination persisted after sputtering (spectrum 6). The true MnO spectrum was obtained by scaling spectrum 6 to align the prepeak (arrow) with spectrum 5, and taking the difference. The resulting spectrum 7 was checked by comparison to EELS O K edge data on MnO from ref 31 (specrtrum 8).

data.[31] The EELS technique is less surface sensitive and, hence, not affected by surface contamination.

The different results at the Mn and O edges after sputtering indicate further oxygen contamination than that associated with Mn_2O_3, but the nature of this species is unknown. Mn K edge data detected no oxidation (seen by agreement with earlier published data and present calculations).

MS Electronic Structure Calculations. The most important chemical characteristic of Mn compounds is the presence of partly occupied 3d orbitals. XANES spectroscopy of these compounds has the interesting characteristic that the K and L absorption edges probe different aspects of the electronic structure and have generally been studied independently. The acquisition of XANES for all relevant edges in these compounds allows each absorption edge to be evaluated for chemical and structural investigations in unknown or complex systems. First, a review is given of the ground-state electronic structure, followed by a description of how this is probed in the X-ray absorption process. We show that a multiple scattering theoretical approach is a valid description of the ground state of these systems. This is then used to simulate experimental XANES, allowing connections to be made to bonding and structural properties. The exception is the Mn L edge, as explained below (the reader is referred to excellent reviews[37−39]).

Ground State. In transition metal oxides, empty or partly filled 3d states are the lowest lying unoccupied states. Mn oxides are magnetic insulators: while band structure considerations would predict a metallic ground state, electron repulsion prevents charge transfer between cation orbitals.[40] The d states are consequently highly localized, and even a pure ionic model reproduces many important aspects of electronic structure. In

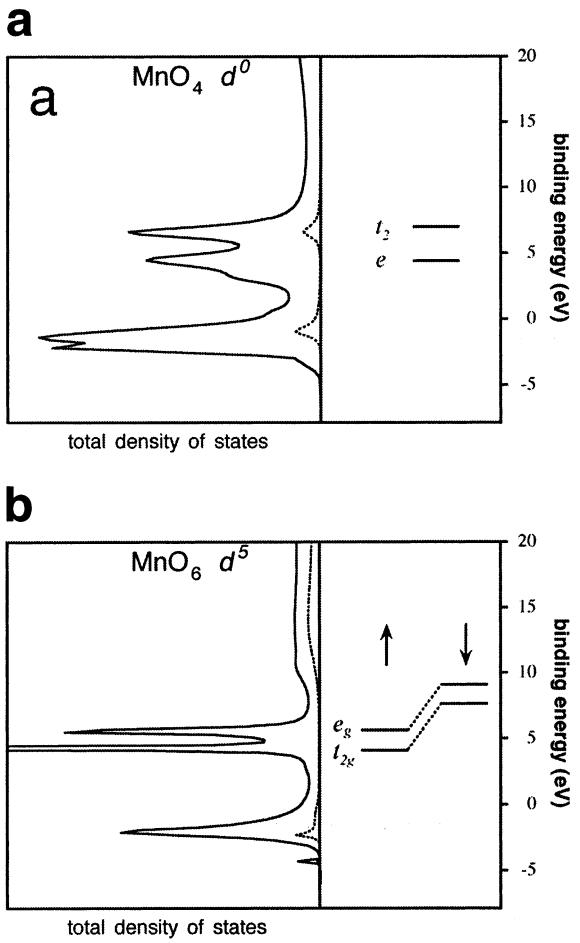

Figure 5. Energy level diagrams of the *3d* valence states (solid lines) of (a**)** Mn O_4 (T_d point group); and (b**)** MnO_6 (O_h point group) clusters calculated by spin independent full multiple scattering (FMS) from spherical muffin tin potentials (this work) and compared with symmetry labeled molecular orbital energy levels (only the LUMO d orbitals are given) from refs 28 and 30. In each case, the crystal field splitting of the d states is well reproduced by the FMS calculations. The p-projected DOS are given by dashed lines, and match the p−d hybridization expected from symmetry principles, as described in the text. For MnO_6, the levels are further split by exchange interactions into spin up and spin down states, which is not reproduced here by the spin independent FMS calculations. In each case, the lowest-lying states from the FMS calculations are occupied metal−ligand sp bonds with some d character.

particular, the ligand crystal field splits the d state energies for specific ligand geometries, whereas interelectron interactions that further reduce degeneracy depend on the occupation of the d states, that is, the oxidation state. Electron exchange interactions impose an energy cost for double electron occupation of a single angular momentum state that is greater than the octahedral crystal field stabilization energy for the Mn 2+, 3+, and 4+ compounds considered here. Consequently all d spins are unpaired, leading to the high spin ground-state configurations given in Table 1.

Figure 5 shows the crystal field splitting of Mn d states in tetrahedral and octahedral geometry, with the present FEFF multiple scattering calculations compared to molecular orbital energy levels (refs 28 and 30) for simple MnO_x ($x = 4,6$) clusters. The electronic ground state in these solids must additionally include band formation with the imposition of crystal periodicity and spin dependent exchange−correlation interaction. The former is approached in FEFF by large cluster calculations, and the exchange splitting of partially occupied states is introduced below.

X-ray Photoexcited State. All information in X-ray absorption spectroscopy relates to the unoccupied electronic states of the photoexcited system. Particular final states are in general "chosen" by the dipole selection rules ($\Delta l = \pm 1$) for a particular absorption edge, although exceptions to these rules are important at transition metal K edges. The lowest energy transitions in X-ray absorption spectra of the manganese oxides are to the partly occupied d states, when allowed. Higher energy transitions are to extended metal−oxygen sp bands. The presence of a core hole after photoexcitation may strongly affect final state energies, especially in insulating specimens. There is a further complication which is difficult to reconcile with band structure approaches: the presence of a manifold of many electron excited states. Following photoexcitation from a core p level to the partially occupied *d* states, d−d and core p-hole d interactions lead to many-electron multiplet states, responsible for rich absorption structure.

These effects are strongest at the Mn L edge, because of the strengths of the white line intensity and the 2p−3d overlap. Atomic multiplet calculations with intermediate coupling has demonstrated that, in transition metal L edge absorption, excitation of the 2p electron gives complex and distinct absorption line shapes representative of the oxidation state because the multiplet structure depends on the d state occupancy.[37] Therefore, Mn L edge spectroscopy can give distinct line shapes associated with specific oxidation states and coordination environments, but bonding parameters such as the crystal field splitting can be difficult to extract.

A similar analysis applies for 1s → 3d transitions (i.e., Mn K edge absorption), but these are dipole forbidden (in the absence of Mn p−d hybridization) and the 1s−3d overlap is small; hence, they are often of extremely weak intensity.[41] By contrast, the lowest energy excitation of the oxygen s electron is of a charge-transfer type, removing the core hole contribution to multiplet states. Oxygen K edge absorption may therefore be a clearer probe of orbital energies, but no firm interpretation of oxygen XAS fine structure has yet been achieved.[32] A better understanding of O K edge absorption and comparison with the Mn K edge are aims of this work.

The present multiple scattering calculations do not give a proper description of multielectron excited states. An effective single particle theory replaces the Hartree−Fock description of a many electron system, and treats a single excited electron interacting with the surrounding system through a local exchange correlation potential. Hence resonances associated with specific electronic configurations are lost, and this approach is unsuited to Mn L edge absorption. However, metal−ligand overlap quickly complicates multiplet analysis. Although atomic multiplet theory is highly successful for very ionic compounds (e.g., MnO), the Mn−O bond covalency increases with Mn valence, and sharp features at the Mn L edge are lost.[17] As we use a single particle theory for the simulation of XANES, electron states are labeled by their orbital symmetry, not spectral terms.

MS Calculations of Mn K edge XANES. *Main Edge.* Spin independent MS code is appropriate to model Mn K main edge absorption, and the agreement between data and calculation is good for all compounds, with the exception of $KMnO_4$. All fine structure in the XANES spectroscopy of the simple oxides is reproduced, although there is some discrepancy in the peak energy positions within approximately 30 eV of the threshold. Shifts in peak energy may be due to inaccuracy in the calculated potentials or the photoelectron self-energy.[33] It was important to calculate absorption at both distinct Mn sites in Mn_2O_3 and Mn_3O_4 (see Table 1) to obtain agreement with data. In all cases, there appears to be a suppression of intensity at the threshold. In particular, the threshold position is about 5 eV too high in energy with respect to the experimental data in the case of $KMnO_4$, and about 3 eV too high for Mn_3O_4, both of which contain some or all Mn atoms in tetrahedral coordination. This discrepancy was not affected by modifying the exchange potential nor by screening the core hole. Instead, the following mechanism may explain the intensity suppression at threshold. The use of spherical potentials underestimates the degree of metal−ligand hybridization, and hence, the strength of charge transfer absorption is likely to be suppressed. This effect would be expected to be more serious with increasing covalency (hence for lower Mn coordination and higher valence) and this is observed as the tetrahedral Mn atoms are more severely affected.

Prepeak. The 1s → 3d prepeak in transition metal K edges is widely used as a sensitive probe of metal atom oxidation state and coordination, despite its relative weakness compared to the full absorption spectrum. Two phenomena, dipole-forbidden quadrupole s−d transitions, and metal atom p−d hybridization, can be responsible for the existence of the prepeak and explain its low intensity. However, the balance of these contributions has been quantified only for a very few systems.[42,43] Orbital symmetry forbids Mn p−d mixing when the Mn site contains a center of inversion (is centrosymmetric), as for the O_h point group, but it may occur in alternative geometries, or in the presence of static distortion,[44] or thermal fluctuations. Quadrupolar transitions do not follow these symmetry selection rules, but are expected to be 10−100 times less intense.[43]

The prepeak acts as a clear indicator of tetrahedral coordination because p−d hybridization is allowed in this geometry, as shown in Figure 5a. In the present data, the prepeak intensity can be correlated with the Mn site symmetry given in Table 1. The strongest Mn K edge prepeak in Figure 2 is associated with tetrahedrally coordinated Mn in $KMnO_4$. There is also a strong component in the Mn_3O_4 spectrum that we attribute to the Mn atoms in tetrahedral coordination.

The spin independent MS calculations of the prepeak are qualitatively in agreement with the data.Transitions to *d* states from Mn core *s* levels are predicted only when there is finite p−d hybridization at the Mn atom. The existence of this hybridization is correctly predicted by FEFF, but neglect of excited state multiplet terms means that the calculated prepeak fine structure is due to crystal field splitting only. The only case in which this gives evident disagreement is MnO_2.

An unexpected result is the observation of an apparent prepeak in the MnO data, which is closely reproduced by calculation. This feature is present in earlier MnO spectra,[20] acquired in fluorescence yield, and is not from contamination. Mn is in perfect O_h symmetry in rocksalt MnO, and according to the above argument, the prepeak should be absent for dipole transitions. Indeed, this is shown in the FEFF calculations of Figure 5b, by the absence of p mixing in the t_{2g}- and e_g- like d states. Quadrupolar transitions would be expected to give a double peak, but only a single peak is detected from the second derivative. To investigate this feature, pre-edge multiple scattering calculations were repeated with the muffin tin potentials and absorption spectrum derived from nearest neighbor oxygen atoms only (i.e., from an embedded MnO_6 cluster). The results gave no preedge feature. By contrast, equivalent nearest neighbor calculations for MnO_4 (in $KMnO_4$) and Jahn−Teller distorted MnO_6 (in MnO_2) reproduced the experimental prepeak. Retaining the same muffin tin potentials, but increasing the full multiple scattering cluster size, the theoretical prepeak emerged

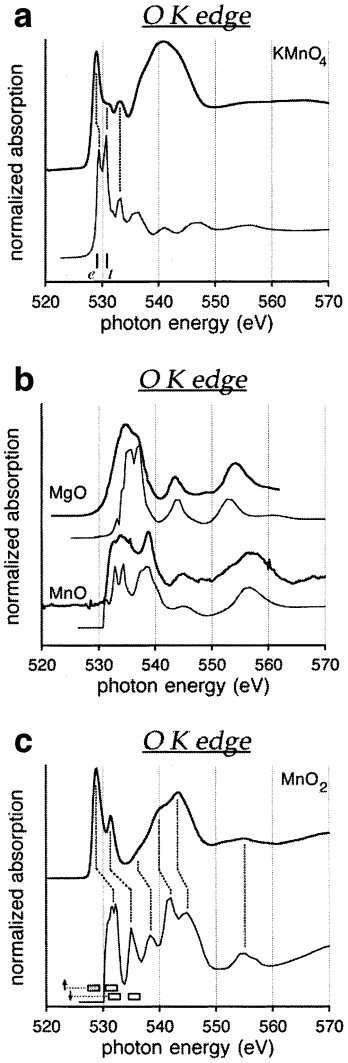

Figure 6. (a**)** Spin independent FMS calculations of oxygen K edge XANES of K MnO_4. (b**)** Spin dependent FMS calculations of oxygen K edge XANES of MnO, compared with spin independent FMS calculations of isostructural MgO. (c**)** Spin dependent FMS calculations of oxygen K edge XANES of MnO_2.

in the MnO system, at a cluster radius of 5.0 Å (at the fifth shell). We therefore conclude that the first feature in the Mn K edge spectrum for MnO is of a different nature than the genuine 1s → 3d prepeaks in $KMnO_4$, MnO_2 and tetrahedral Mn in Mn_2O_3, and is instead a result of the transition 1s → continuum, including long-range photoelectron scattering. The coincidence of the photon energy of this feature and the prepeaks of the other materials is accidental, because of shifts in the energy positions of the Mn 1s and conduction band as the oxidation state of Mn varies.

MS Calculations of O K Edge XANES. We consider the transition $d^n \rightarrow (Ls^1)d^{n+1}$, where this excitation is permitted due to the hybridization of ligand p and Mn d states, and Ls^1 = ligand s level hole. For partially filled d levels, we calculate separately the electronic density of states and then sum the normalized partial X-ray absorption cross sections for the spin-up and -down cases.

$KMnO_4$. As the LUMO d levels are empty, there is no associated exchange splitting, so this system is appropriate for a spin independent multiple scattering approach. The oxygen near edge absorption is given in Figure 6a, compared to the FMS calculations and the relative positions of the Mn 3d-derived e and t antibonding orbitals from Figure 5a. Hence, the first two peaks are transitions to e and t states, reproduced by calculation but with incorrect relative intensities. The third peak is a multiple scattering feature, which emerges at the third shell. There is poor agreement with the broad resonance post threshold. In analogy with carbon 1s spectroscopy,[45] this feature is attributed to a linear Mn−O σ^* antibonding orbital, which are poorly represented by FEFF.

MnO. The most striking observation for the O K edge for MnO is that the threshold of absorption is shifted by several eV to higher energy than for all other compounds (Figure 3). Spin independent FMS calculations for MnO (not shown) cannot reproduce this shift but do give good agreement for MgO, as shown in Figure 6b. It is clear from the spin dependent molecular orbital calculations of Figure 5b that the apparent shift occurs because the spin down exchange split bands are completely occupied.

The results of spin dependent MS calculations are given in Figure 6b, with the relative positions of the unoccupied spin up d bands derived from the spin dependent calculation. Only two final states are possible: $[(t_{2g})^3\uparrow(e_g)^2\downarrow(t_{2g})^1]$ and $[\uparrow(t_{2g})^3\uparrow(e_g)^2\downarrow(e_g)^1]$ (neglecting excited states requiring simultaneous Mn d−d transitions). Nevertheless, the line shape is broad, and the expected contributions are not resolvable in the experimental spectrum. Extra structure in the equivalent spectral region for NiO has been interpreted as being of a multielectron nature, because of configuration interaction between the Ni 3d bands and the O valence 2p electrons.[46]

MnO_2. Calculated and experimental spectra of MnO_2 are given in Figure 6c, with the relative positions of the spin up and spin down d bands. The exchange and crystal field splittings are similar in magnitude, leading to the doublet in the oxygen near edge, despite the possibility of three d^{n+1} final states: $[\uparrow(t_{2g})^3\downarrow(t_{2g})^1]$; $[\uparrow(t_{2g})^3\uparrow(e_g)^1]$; $[\uparrow(t_{2g})^3\downarrow(e_g)^1]$ (the slight Jahn Teller distortion to lower symmetry is neglected). The calculations demonstrate the accidental degeneracy of the lowest energy excited states and justify the observation of previous authors that the oxygen near edge splitting is close to the 10Dq value of the crystal field splitting.[32] The calculated peak separations are less than observed, but there is good overall fine structure agreement.

Discussion

Empirical Trends and Fingerprints. Individual absorption line shapes may act as fingerprints for specific species in complex specimens, and trends in absorption line shapes and positions are often of aid in understanding poorly characterized specimens.

Shifts with Mn Valence. The threshold position of transition metal K edges shift to higher energy with increasing metal valence. The threshold represents transitions to antibonding metal ligand σ bonds. For a given geometry, as the cation oxidation state increases, the bonding orbitals are more tightly bound and antibonding orbitals are consequently higher in energy. A linear relationship has been shown for nickel and vanadium, with shifts of, respectively, 1.5 or 2.5 eV per unit increase in valence.[47,48] The corresponding shifts for Mn are given in Figure 7 and are not linear, especially when the 7+ valence state is included. However, covalent effects reduce the charge at the Mn atom, and consequently, the rise in anti bonding levels does not follow the formal valence. A more linear relationship is observed when the manganese charge transfer calculated self-consistently by the FEFF code is used in place of the formal valence. The difference in the two plots is a record of the increasing covalency as formal valence increases. A

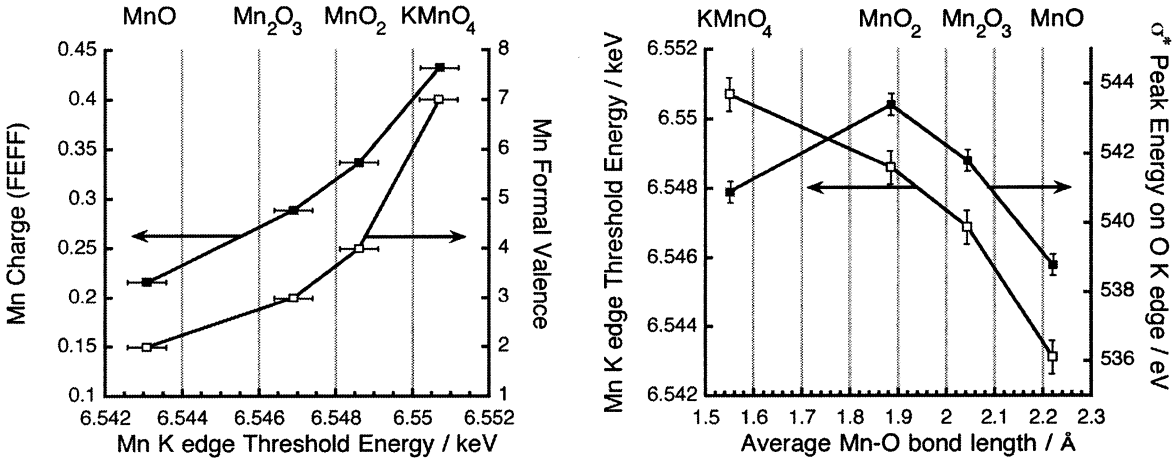

Figure 7. (a) Shift in the energy position of the Mn K edge threshold absorption, plotted versus the formal Mn valence, and the charge transfer, calculated self-consistently for muffin tin potentials by the FEFF code. (b) For octahedrally coordinated Mn, the shift of the Mn K edge threshold and of the σ^* resonance in the O K absorption are linked, as they represent transitions to the same final state. This is clearly seen by plotting them together versus the average Mn−O bond length, as explained in the text.

similar trend has been shown at the Mn L edge, for which white line intensities are fairly proportional to the formal 3d occupation, but the relationship improves when covalency is considered.[31]

There is clearly no simple trend in threshold positions at the oxygen K edge, and in particular, the onset of absorption is more than 3 eV higher in energy for MnO than all other compounds. However, trends in Mn and O K edge absorption can be linked. As shown by FEFF calculations, O K edge absorption involves transitions to metal sp−ligand p states, the same final states at threshold at Mn K edges. From molecular orbital considerations, these σ antibonding orbitals are sensitive to the metal−ligand bond length. Unlike estimates of valence or charge transfer, bond lengths are accurately determined (Table 1), so Figure 7 shows the trend in σ^* peak positions with Mn−O average bond length compared to the trend in Mn K edge threshold positions. There is a clear agreement in the trends for all compounds containing octahedrally coordinated Mn.

Structural Fingerprints. *1. Nearest Neighbor Geometry from Bound Unoccupied Levels.* XANES line shapes at certain edges are frequently encountered that are characteristic of local absorber geometry, which splits the electronic energy levels in a repeatable way. This and the additional splitting of 3d energy levels due to spin occupation gives Mn L edge line shapes for (i) local coordination, (ii) occupation (oxidation state), and (iii) spin arrangement that are also distinct and repeatable.[37,39] Hence, multiple components are separable from complex mixtures (e.g. Figure 4), and the spectra from mixed valence compounds (e.g., Mn_3O_4) are equivalent to the sum of individual valence references, provided local geometry is taken into account. However, Mn oxidation state is the greatest factor determining the line shape, and there has been no systematic experimental study on the sensitivity of the Mn L edge to lower site symmetries than pure T_d or O_h. Also, although experimental studies have shown that the Mn 2+ line shape is consistent for many ligands[17] for a given geometry, similar investigations are lacking for the higher valences.

2. Nearest Neighbor Geometry from Continuum Scattering. Just as nearest neighbor geometry affects bound unoccupied states, particular scattering pathways give rise to resonances associated with local symmetry. This is clearly shown in the comparison between MnO and MgO at the O K edge, which have very similar line shapes above threshold. The FMS calculations show that the line shape is mainly due to nearest neighbors in the rock salt crystal, with extra contributions from farther shells.

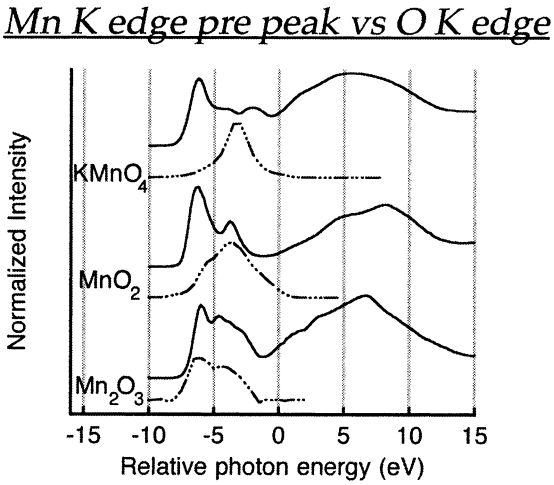

Figure 8. Comparison of Mn K edge pre peak and O K near edge fine structure, by rigidly shifting the extracted Mn pre peak and O spectra onto a common relative energy scale.

3. Medium Range Crystal Geometry from Multiple Scattering Resonances. The photoabsorption process is also sensitive to the extended structure beyond nearest neighbors. Although the strength of the white line absorption obscures this information at the Mn L edge, the Mn and O K edges are sensitive to crystal structure up to a radius of 5.7−8.0 Å. A value on the material length-scale probed by the X-ray absorption process is an extremely important parameter for the study of reduced dimension materials. An understanding of contributions from beyond the first shell is possible only by combining experiment and FMS cluster calculations.[25]

Comparison of Mn K Edge Prepeak and O K Edge XANES. We qualitatively compare the relative ability of the Mn K edge prepeak and O K near edge absorption to probe 3d orbital energies by plotting them in Figure 8 on a common relative energy scale. The Mn prepeak has been isolated from the full K edge spectrum by subtracting a cubic spline fit to threshold, excluding the prepeak region. For Mn and O K edges, d^{n+1} multielectron final states are expected (we neglect those requiring double electron excitation). However, O K edge absorption is of charge-transfer nature, so fewer symmetry restrictions allow more transitions, and there is negligible overlap

between core hole and excited d states. In addition, lower core hole broadening results in sharper absorption structure.

These expectations are most clearly realized for $KMnO_4$: the first two peaks in the oxygen spectrum represent transitions to the t and e antibonding states; only the t transition is allowed at in the Mn spectrum due to Mn p−d hybridization in this level alone (see Figure 5a).

For MnO_2, three peaks are resolvable in the Mn prepeak, whereas only a clear doublet is observed for oxygen (explained above). There are several possibilities for the discrepancy at the Mn K edge: (i) the presence of the Mn 1s core hole induces further multiplet splitting in the final state; (ii) the Mn 1s core hole modifies the energies of the final states, removing the accidental degeneracy of the lowest energy excited states. In fact, spin dependent MS calculations, which are successful at the O K edge, show that final state energies are negligibly affected by the presence of the core hole and give poor results for the Mn prepeak. Therefore, we conclude that fine structure at the Mn K edge prepeak cannot be reproduced without considering multiplet interactions.

The situation for Mn_2O_3 is more complicated because there are two distinct Mn sites, and the Mn K edge prepeak closely resembles the O near edge structure, with the expected additional broadening. Nevertheless, we maintain the previous conclusion that the Mn K edge prepeak fine structure is influenced by multiplet interactions, and the O K edge gives the better description of valence states.

Role of Calculations in Data Analysis and Interpretation. It is clear from Figures 2 and 6 that the agreement obtained between data and calculation is variable, even for the materials considered here. However, many discrepancies can be anticipated, and hence, theoretical calculations may be of value in more complex systems as long as plausible structural models are available. Disagreement in peak position is often systematic, whereas errors in peak amplitudes may be expected, as the use of Debye−Waller factors to represent thermal disorder is not accurate for multiple scattering. Closer to the threshold, neglect of nonspherical contributions can also lead to inaccurate peak intensities. Finally, the absolute value of the exchange splitting will be incorrect for some materials. These limitations indicate that the present MS calculations may predict fairly well the contributions to X-ray absorption structure (with the exception of multiplet states) but with inaccurate absolute energy positions or intensities. In XANES spectroscopy, unlike the situation for EXAFS, theoretical calculations are far from being able to replace empirical references.

Manganese oxide perovskites typically possess very rich structural and electronic phase diagrams and provide an excellent example of the sensitivity of XANES to both physical and electronic structure, and of the use of MS calculations, despite the above limitations. Manganese valence can be detected at the Mn L edge,[4] local structure modifications at the Mn K edge,[4] and electronic contributions or hybridization at the O K edge.[3,49] MS calculations allow structural models to be assessed or the presence of metal ion−dopant hybridization to be tested.

4. Conclusions

XANES of manganese oxides can be divided into three regimes: 1. transitions to exchange split *d* states; 2. transitions to covalent metal sp−oxygen p antibonding states at the conduction band minimum; 3. transitions to higher energy conduction bands. These are probed to different degrees by the separate X-ray absorption edges of manganese and oxygen, which have then different strengths for chemical and structural investigations. Mn L edge absorption is completely dominated by Mn 3d states (regime 1) and, hence, is an excellent indicator of Mn oxidation state and coordination.

The Mn K edge probes regime 3 (above threshold) and hence is an excellent short to medium range structural probe. Spin independent multiple scattering calculations accurately model this regime. This edge is not a good probe of metal−oxygen bonding, as the strongest transitions are to empty Mn p states, rather than the antibonding states associated with this bond. The Mn K edge prepeak probes regime 1, and the strength of the prepeak is qualitatively modeled by spin independent calculations as a result of Mn d−O p hybridization.

This approach reveals that the apparent prepeak for MnO is actually the result of low energy photoelectron scattering up to the fifth shell. Solid-state contributions to XANES, that is, fine structure associated with photoelectron scattering from beyond the nearest neighbor shell, are important at the Mn and O K edges.

Spin dependent calculations are essential for simulations at the oxygen K edge for compounds with partly occupied d states. Within around 5 eV of threshold, the final states are exchange split d states, which are well modeled by spin dependent calculations. Higher energy absorption fine structure is reproduced, including transitions to sp hybrid orbitals, with the exception of $KMnO_4$. Despite good agreement at the O K edge, spin dependent MS calculations were not sufficient to reproduce the fine structure within the Mn K edge prepeak, and we conclude that multiplet interactions cannot be neglected. By contrast, final state multiplet interactions are negligible for O K edge absorption, and hence, this edge is the clearest probe of bonding in the manganese oxides.

The results for multiple scattering calculations were consistently poorer for $KMnO_4$ than the other compounds studied. We interpret this as being due to the highly directional covalent bonds in the MnO_4 species, because such bonds are poorly reproduced by muffin tin potentials.

Our calculations indicate that the presence of an oxygen core hole has little effect on the absorption spectrum; hence, we anticipate that a full potential spin dependent ground state DOS calculation would be a valuable approach for further interpreting the near edge fine structure of oxygen in magnetic insulators. Overall, this work gives a coherent picture of bonding and X-ray absorption spectroscopy in the manganese oxides and describes the accuracy presently attained by multiple scattering calculations.

Acknowledgment. We acknowledge the support of the University of Wisconsin Graduate School, Physics Department, University−Industry Relations and the Comprehensive Cancer Center. X-ray absorption spectroscopy was performed at the Wisconsin Synchrotron Radiation Center, a facility supported by NSF under Grant DMR-95-31009, and the Advanced Photon source, a facility supported by the U.S. Department of Energy, Office of Science, Office of Basic Energy Sciences under Contract No. W-31-109-ENG-38. We thank Mark Bissen and the staff at SRC. Thanks to Jill Banfield and Michael Finnegan for use of the X-ray diffractometer.

References and Notes

(1) Ammundsen, B.; Jones, D. J.; Roziere, J. *J. Solid State Chem.* **1998**, *141*, 294.

(2) Ignatov, A. Y.; Ali, N.; Khalid, S. *Phys. Rev. B* **2001**, *64*, 014413.

(3) Saitoh, T.; Bocquet, A. E.; Mizokawa, T.; Namatame, H.; Fujimori, A.; Abbate, M.; Takeda, Y.; Takano, M. *Phys. Rev. B* **1995**, *51*, 13942.

(4) Sanchez, M. C.; Garcia, J.; Blasco, J.; Subias, G.; Perez-Cacho, J. *Phys. Rev. B* **2002**, *65*, 144409.
(5) Grush, M. M.; Chen, J.; Stemmler, T. L.; George, S. J.; Ralston, C. Y.; Stilbrany, R. T.; Gelasco, A.; Christou, G.; Gorun, S. M.; Penner-Hahn, J. E.; Cramer, S. P. *J. Am. Chem. Soc.*, **1996**, *118*, 65.
(6) Bargar, J. R.; Tebo, B. M.; Villinski, J. E. *Geochim. Cosmochim. Acta* **2000**, *64*, 2775.
(7) McKeown, D. A.; Post, J. E. *Am. Mineral.* **2001**, *86*, 701.
(8) Manceau, A.; Gorshkov, A. I.; Drits, V. A. *Am. Mineral.* **1992**, *77*, 1133.
(9) Chen, W.; Sammynaiken, R.; Huang, Y.; Malm, J.-O.; Wallenberg, R.; Bovin, J.-O.; Zwiller, V.; Kotov, N. A. *J. Appl. Phys*. **2001**, *89*, 1120.
(10) Tebo, B. M.; Ghiorse, W. C.; van Waasbergen, L. G.; Siering, P. L.; Caspi, R. Reviews in Mineralogy. In *Geomicrobiology: interactions between microbes and minerals*; Banfield, J. F., Nealson, K. H., Eds.; Mineralogy Society of America: Washington, 1997; Vol. 35.
(11) Shibata, T.; Bunker, B.; Mitchell, J. F.; Schiffer, P. *Phys. Rev. Lett.* **2002**, *88*, 207205.
(12) De Stasio, G.; Gilbert, B.; Frazer, B. H.; Nealson, K. H.; Conrad, P. G.; Livi, V.; Labrenz, M.; Banfield, J. F. *J. Elec. Spec. Relat. Phenom.* **2001**, *114*, 997.
(13) Labrenz, M.; Druschel, G. K.; Thomsen-Ebert, T.; Gilbert, B.; Welch, S. A.; Kemner, K. M.; Logan, G. A.; Summons, R. E.; De Stasio, G.; Bond, P. L.; Lai, B.; Kelly, S. D.; Banfield, J. F. *Science* **2000**, *270*, 1744.
(14) Meyer-Ilse, W., Warwick, T., Attwood, D., Eds.; *X-ray Microscopy. AIP Conference Proceedings 507*; AIP: Melville, NY, 2000.
(15) Maser, J.; Osanna, A.; Wang, Y.; Jacobsen, C.; Kirz, J.; Spector, S.; Winn, B.; Tennant, D. *J. Microscopy−Oxford* **2000**, *197*, 68.
(16) Frazer, B. H.; Gilbert, B.; De Stasio, G. *Rev. Sci. Instrum*. **2002**, *73*, 1373.
(17) Cramer, S. P.; de Groot, F. M. F.; Ma, Y.; Chen, C. T.; Sette, F.; Kipke, C. A.; Eichhorn, D. M.; Chan, M. K.; Armstrong, W. H.; Libby, E.; Christou, G.; Brooker, S.; McKee, V.; Mullins, O. C.; Fuggle, J. C. *J. Am. Chem. Soc.* **1991**, *113*, 7937.
(18) Garvie, L. A. J.; Craven, A. J. *J. Phys. Chem. Minerals* **1994**, *21*, 191.
(19) Apte, M. Y.; Mande, C. *J. Phys. Chem. Solids* **1980**, *41*, 307.
(20) Belli, M.; Scafati, A.; Bianconi, A.; Mobilio, S.; Palladino, L.; Reale, L.; Burattini, E. *Solid State Commun.* **1980**, *35*, 355.
(21) Tonner, B. P.; Droubay, T.; Denlinger, J.; Meyer-Ilse, W.; Warwick, T.; Rothe, J.; Kneedler, E.; Pecher, K.; Nealson, K.; Grundl, T. *Surf. Interface Anal.* **1999**, *27*, 247.
(22) Nakai, S.; Mitsuishi, T.; Sugawara, H.; Maezawa, H.; Matsukawa, T.; Mitani, S.; Yamasaki, K.; Fujikawa, T. *Phys. Rev. B* **1987**, *36*, 9241.
(23) Kawai, J.; Mizutani, Y.; Sugimura, T.; Sai, M.; Higuchi, T.; Harada, T.; Ishiwata, Y.; Fukushima, A.; Fujisawa, M.; Watanabe, M.; Maeda, K.; Shin, S.; Gihshi, Y. *Spectrochim. Acta B* **2000**, *55*, 1385.
(24) Ankudinov, A.; Ravel, B.; Rehr, J. J.; Conradson, S. D. *Phys. Rev. B* **1998**, *58*, 7565.
(25) Gilbert, B.; Frazer, B. H.; Zhang, H.; Huang, H.; Banfield, J. F.; Haskel, D.; Lang, J. C.; Srajer, G.; De Stasio, G. *Phys. Rev. B* In press.
(26) Wyckoff, P. *Crystal Structures*; Wiley: New York, 1963.
(27) Farges, F.; Brown, G. E., Jr.; Rehr, J. J. *Geochim. Cosmochim. Acta* **1996**, *60*, 3023.
(28) Sherman, D. M. *Am. Mineral.* **1984**, *69*, 788.
(29) Soldatov, A. V.; Ivanchenko, T. S.; Kovtun, A. P.; Della Longa, S.; Bianconi, A. *Phys. Rev. B* **1995**, *52*, 11757.
(30) Di Bartolo, B. *Optical interactions in solids*; John Wiley & Sons: New York, 1968.
(31) Kurata, H.; Colliex, C. *Phys. Rev. B* **1993**, *48*, 2102.
(32) de Groot, F. M. F.; Grioni, M.; Fuggle, J. C.; Ghijsen, J.; Sawatzky, G. A.; Petersen, H. *Phys. Rev. B* **1989**, *40*, 5715.
(33) Rehr, J. J.; Albers, R. C. *Rev. Mod. Phys.* **2000**, *72*, 621.
(34) Kostlmeier, S.; Elsasser, C. *Phys. Rev. B* **1999**, *60*, 14025.
(35) Kurata, H.; Lefevre, E.; Colliex, C.; Brydson, R. *Phys. Rev. B* **1992**, *47*, 13763.
(36) Murray, J. W.; Dillard, J. G.; Giovanoli, R.; Moers, H.; Stumm, W. *Geochim. Cosmochim. Acta* **1985**, *49*, 463.
(37) de Groot, F. M. F.; Fuggle, J. C.; Thole, B. T.; Sawatzky, G. A. *Phys. Rev. B* **1990**, *42*, 5459.
(38) de Groot, F. M. F. *Chem. Rev.* **2001**, *101*, 1779.
(39) van der Laan, G.; Kirkman, I. W. *J. Phys. Condens. Matter* **1992**, *4*, 4189.
(40) Cox, P. A. *Transition Metal Oxides: An Introduction to their Electronic Structure and Properties*; Clarendon Press: Oxford, 1997.
(41) de Groot, F. M. F. *J. Elec. Spec. Relat. Phenom.* **1994**, *67*, 529.
(42) Westre, T. E.; Kennepohl, P.; Dewitt, J. G.; Hedman, B.; Hodgson, K. O.; Solomon, E. I. *J. Am. Chem. Soc*. **1997**, *119*, 6297.
(43) Boulder, C. *J. Phys.: Condens. Matter* **1990**, *2*, 701.
(44) Waychunas, G. A. *Am. Mineral.* **1987**, *72*, 89.
(45) Stohr, J. *NEXAFS spectroscopy*; Springer-Verlag: Berlin, 1996.
(46) Davoli, I.; Marcelli, A.; Bianconi, A.; Tomellini, M.; Fanfoni, M. *Phys. Rev. B* **1986**, *33*, 2979.
(47) Mansour, A. N.; Melendres, C. A. *J. Phys. Chem. A* **1998**, *102*, 65.
(48) Wong, J.; Lytle, F. W.; Messmer, R. P.; Maylotte, D. H. *Phys. Rev. B* **1984**, *30*, 5596.
(49) Ju, H. L.; Sohn, H.-C.; Krishnan, K. M. *Phys. Rev. Lett*. **1997**, *79*, 3230.